11

Ion Beam Neutralization

It is more difficult to transport high-current ion beams than electron beams. Nonrelativistic ions move slower than electrons of equal kinetic energy. Therefore an ion beam has higher space-charge electric fields than an electron beam of the same current. Also magnetic focusing by beam-generated fields is ineffective for nonrelativistic beams. We must apply neutralization to create and to transport high-flux ion beams. The idea is to mix electrons with the ions to reduce the beam-generated electric field. The process is feasible because of the low mass of the electron. The mobile electrons rapidly enter the beam volume. Low-energy electrons can follow high-energy ions to neutralize a beam propagating into free space. Also the technology to generate electrons is straightforward compared with the complexity of ion sources (Chapter 7).

There are two ways to neutralize an ion beam with electrons. First, we can direct the beam through a dense plasma. The plasma electrons shift in position to compensate for the added positive charge. Plasma neutralization is an important process for large-area ion extractors that use a gas-injection plasma source. The beam ionizes gas leaking from the source to produce a high-density, low-temperature plasma. Although this neutralization method has practical importance, we shall not address it in this chapter. The characteristics of the plasma depend on complex collisional processes. Prediction of the plasma properties and residual electric fields involves applied plasma and atomic physics rather than beam theory.

In this chapter, we shall concentrate on an alternative approach, *vacuum neutralization*. Here, sources located outside the vacuum beam transport region create the electrons. The electrons join the ions as needed. The resulting neutralized beam has an electron density approximately equal to the beam density. Collisions with the electrons have little effect on the ion trajectories. Therefore, beams neutralized by externally-generated electrons can propagate long distances.

Section 11.1 describes longitudinal neutralization where electrons follow an ion beam entering a field-free vacuum. There are two options for the generation of collinear electrons. The first is to accelerate the electrons to the ion velocity by an electric applied field. The second is to allow the space-charge field of the beam to attract electrons. We shall show that the latter method of passive neutralization results in an electron distribution with a density and average velocity equal to that of the ions. Section 11.2 treats a similar process where electrons enter the side of the

beam in response to space-charge electric fields. This model applies to ion beams in magnetic quadrupole lenses or bending magnets where the fields prevent the axial motion of electrons. Section 11.3 describes propagation of an ion beam in a bounded field-free region where electrons neutralize space charge fields but do not cancel the beam current. This effect can be useful for flux measurements of neutralized ion beams.

One motivation for neutralization is to achieve tightly-focused ion beams. With complete cancellation of space-charge fields, only emittance limits the focal spot of an intense beam. Section 11.4 shows that an ideal focus does not occur if the neutralizing electrons have a non-zero temperature. The electric fields generated by electron thermal motion can reach high values in a converging beam, defocusing the ions. To conclude the chapter, Section 11.5 reviews the control of neutralizing electrons with applied magnetic fields to guide and to accelerate ion beams.

11.1. Neutralization by co-moving electrons

In this section, we study the propagation of neutralized ion beams in free space with no applied electric and magnetic fields. Figure 11.1*a* shows the ideal neutralized beam. The electron and ion densities are equal so there is no beam-generated electric field. The electrons move at same velocity as the ions, $v_e = v_i$. The conditions of equal densities and equal velocities imply that the current densities of electrons and ions have equal magnitude but opposite direction. The net current is zero, so there is no beam-generated magnetic field. If T_i is the ion kinetic energy, electrons with equal velocity have kinetic energy:

$$T_e = m_e v_i^2/2 = (m_e/m_i)\, T_i. \tag{11.1}$$

The electron energy is much smaller than T_i. For example, electrons moving with 1 MeV protons have $T_e = 540$ eV. The problem we shall address in this section is how to create a neutralized beam like that of Figure 11.1*a*. We limit attention to longitudinal neutralization where electrons enter the transport region at the same location as the ions and travel in the same direction.

One option for neutralization is to accelerate electrons to kinetic energy T_e and combine them with the ion beam. This process is called *active neutralization*. We shall analyze the process with a one-dimensional model. Figure 11.1*b* illustrates the geometry. Ions with kinetic energy T_i pass through a set of grids. A cathode grid acts as an unlimited source of electrons. If the voltage difference between the grids is

$$V_o = (m_e/m_i)T_i/e, \tag{11.2}$$

electrons reach the anode grid with velocity equal to that of the ions. The electric field between the grids has a negligible effect on the velocity of energetic ions. Therefore, the ions have constant density n_o and velocity $(v_i = (2T_i/m_i)^{1/2})$ throughout the acceleration and propagation regions.

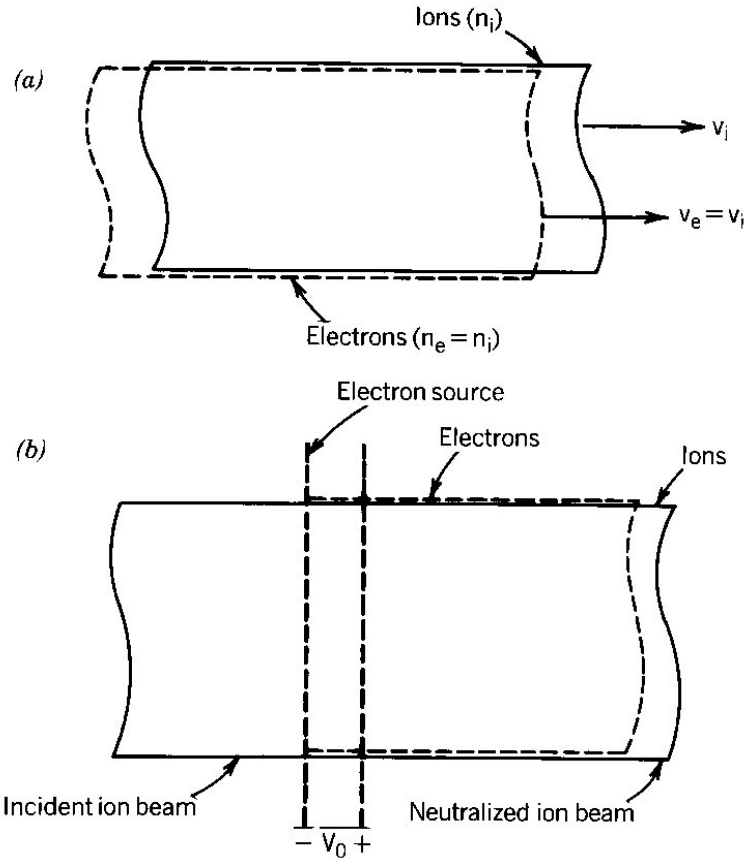

Figure 11.1. Ion beam neutralization. *a*) Ideal neutralized beam - ions and electrons have equal densities and velocities. *b*) Active neutralization - acceleration of electrons to match the density and velocity of the ion beam.

Ideal neutralization results if the magnitude of the electron current density at the anode equals the ion current density, $en_o v_i$. We are free to choose the spacing between grids to achieve this condition. Again, we seek a one-dimensional self-consistent equilibrium for electron flow. The main difference from previous analyses is the inclusion of a uniform ion density. The following boundary conditions hold for a steady-state solution:

1. The electrostatic potential of the cathode (at $z = 0$) is $\phi(0) = 0$.

2. The anode at $z = d$ has potential $\phi = V_o = T_i (m_e/m_i)/e$.

3. Space-charge-limited electron emission reduces the electric field at the cathode to zero, $d\phi(0)/dx = 0$.

4. The electron density equals the ion density at the gap exit, $n_e(x=d) = n_o$.

The one-dimensional Poisson equation that satisfies the boundary conditions is

$$\frac{d^2\phi}{dx^2} = \frac{en_o}{\epsilon_o}\left[\left(\frac{V_o}{\phi}\right)^{1/2} - 1\right]. \tag{11.3}$$

Following the method of Section 6.4, we can show that the electron current density is given by

$$j_e = \frac{4\epsilon_o}{9}\left[\frac{2e}{m_e}\right]^{1/2}\frac{V_o^{3/2}}{d^2}\,G\,, \tag{11.4}$$

where

$$G = \left[\frac{3}{2\sqrt{2}}\int_0^1 \frac{dX}{(2X^{1/2}-X)^{1/2}}\right]^2 = 1.46\,.$$

Because of the ion space-charge, the electron current density is slightly higher than the single-species Child limit [Eq. (5.48)].

As an example of the characteristics of an electron acceleration gap for ion beam neutralization, suppose we have a 100 keV deuteron beam with current density 1×10^4 A/m^2. The neutralizing electrons have kinetic energy $T_e = 27$ eV. The acceleration gap must be very narrow to generate the required electron current-density at low energy, $d = 0.22$ mm. The fundamental problem of active neutralization is the creation of high current density electron flux from a structure that transmits a high-intensity ion beam with little attenuation. Although the one-dimensional mathematical solution is straightforward, the technological realization is quite difficult.

A more practical way to reduce space-charge forces in an ion beam is through *auto-neutralization*. In this process, the space-charge potential of the ion beam accelerates electrons from a grounded surface. Figure 11.2 illustrates a one-dimensional geometry to describe the process. An ion beam of infinite transverse extent leaves a planar surface at $z = 0$. The region $z > 0$ is a field-free volume. The surface at $z = 0$ supplies an unlimited electron flux. The acceleration of electrons by the ion space-charge is a self-limiting process. We recognize that even a small imbalance of charge in an intense ion beam results in a high value of space-charge potential, $\phi \gg (m_e/m_i)T_i/e$. If the electron density is less than that of the ion beam, the resulting electric fields draw more electrons into the beam. An equilibrium occurs when electrons move

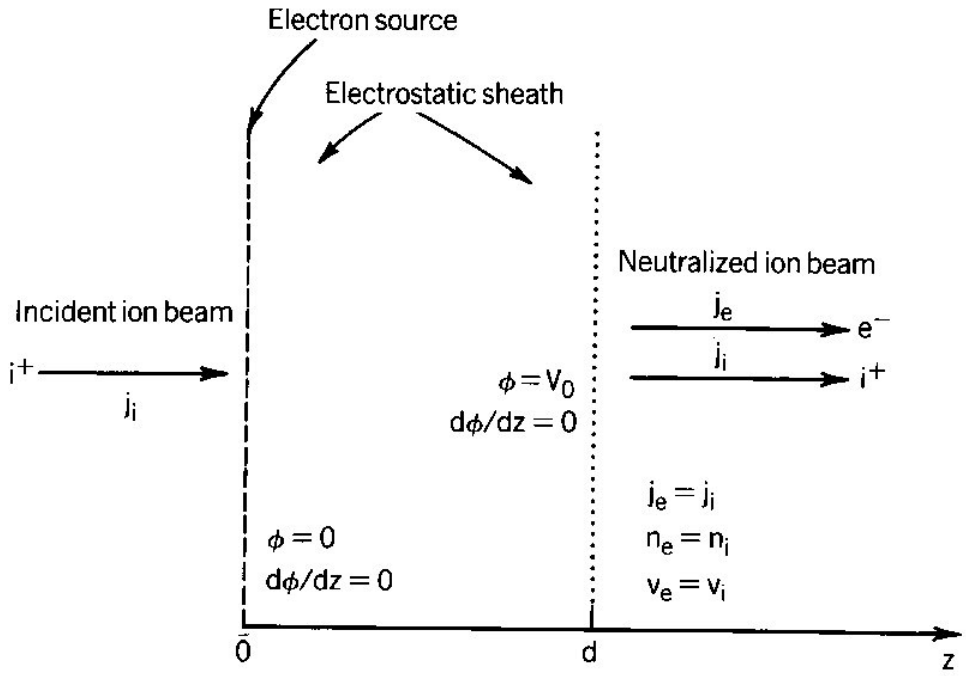

Figure 11.2. Hypothetical desired conditions for ion beam neutralization through space-charge acceleration of electrons.

into the propagation region at the same rate as the ions.

Figure 11.2 illustrates the desired equilibrium solution for auto-neutralization. The space-charge fields accelerate electrons in a thin sheath to match the velocity of the ions. We assume that the sheath occupies the region $0 \le z \le d$. Several conditions constrain the solution of the Poisson equation:

1. The voltage drop across the sheath equals $(m_e/m_i)T_i/e$.

2. The electron current density at $z = d$ equals the ion current density, $j_e = j_o = en_o v_i$.

3. The electric field at $z = 0$ must equal zero because the electron flow is space-charge limited, $d\phi(0)/dz = 0$.

4. The electric field at the sheath exit equals the field inside the propagating beam because there is no charge layer at d. By the assumption of a neutralized beam, $d\phi(d)/dz = 0$.

There are too many boundary conditions for a solution of the Poisson equation. In order to have zero electric field at both sides of the sheath, the potential must follow an S-shaped curve with both positive and negative inflection. The dual inflection occurs only if the ion density exceeds the electron density near $z = d$ and the electron density is larger near $z = 0$. Condition 2 implies

that the electron and ion densities are equal at $z = d$; furthermore, we know that $n_e \sim 1/\phi^{1/2}$ in steady-state. The implication is that the electron density is higher than the ion density everywhere in the sheath.

We must seek solutions with different boundary conditions to explain how auto-neutralization works. One possibility is to look for a steady-state solution where variations of the potential are not contained to a sheath but extend to infinity. For any potential variation, the electron density has the form:

$$n_e(z) = \frac{A}{\sqrt{2e\phi(z)/m_e}} . \tag{11.5}$$

We retain the condition of uniform ion density n_o and current density j_o. To ensure that the electron and ion fluxes are equal, the constant A in Eq. (11.5) has the value $(j_o/e)(2eV_o/m_e)$. In the region $z \geq 0$, the Poisson equation is:

$$\frac{d^2\phi}{dz^2} = \frac{j_o}{\epsilon_o}\left[\left(\frac{V_o}{\phi}\right)^{1/2} - 1\right] . \tag{11.6}$$

We can simplify Eq. (11.6) by defining the dimensionless variables:

$$\Phi = \phi/V_o. \tag{11.7}$$

$$Z = z/(V_o\epsilon_o/en_o)^{1/2}. \tag{11.8}$$

The reduced Poisson equation is:

$$\frac{d^2\Phi}{dZ^2} = \frac{1}{\sqrt{\Phi}} - 1 . \tag{11.9}$$

If emission of electrons from the surface at $Z = 0$ is space-charge limited, the boundary conditions for the solution of Eq. (11.9) are $\Phi(0) = 0$ and $d\Phi'(0)/dZ = 0$. A dual integration of the equation leads to the solution:

$$Z = \sqrt{2}\left[\sin^{-1}(\Phi^{1/2}-1) - [\Phi^{1/2}(1-\Phi^{1/2}/2)]^{1/2} + \pi/2\right] . \tag{11.10}$$

Figure 11.3 illustrates the spatial variation of $\Phi(Z)$. The potential is periodic with values between $\Phi = 0$ and $\Phi = 4$. The distance from the cathode to the first potential maximum is $Z = (2)^{1/2}\pi$. The electrons over-neutralize and under-neutralize the beam. The electron velocity varies

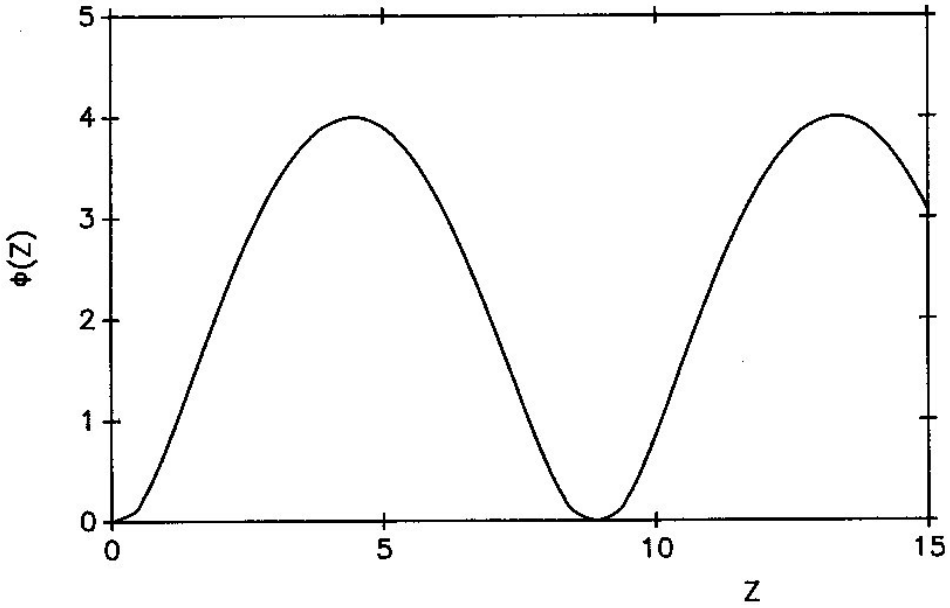

Figure 11.3. Ion beam neutralization by space-charge acceleration of electrons. Steady-state solution when a uniform ion beam occupies the entire region $Z > 0$. $\Phi = \phi/V_o$, $Z = z/(V_o\epsilon_o/en_o)^{1/2}$.

between $v_e = 0$ and $v_e = 2v_i$.

We might conclude from the solution of Eq. (11.10) that effective auto-neutralization is impossible. To explain experimental observations, we recognize that the derivation proceeds from two questionable conditions:

1) The model assumes that an equilibrium state exists in the full half plane $z > 0$ for all times. It ignores processes that may occur as ions and electrons fill the propagation region.

2) The model takes electron motion as purely one-dimensional. The electrons have a delta-function distribution in longitudinal energy.

Regarding the second assumption, we recognize that neutralization is a disordering process where electrons join with ions to form a homogeneous mixture. If we limit motion to one dimension, we may have set an artificial constraint that prevents the electron distribution from attaining thermodynamic equilibrium.

We shall develop a model to show that there are alternative equilibrium solutions that give auto-neutralization with a well-defined sheath region. We include time-dependent processes as an ion beam fills the vacuum propagation region $z \geq 0$. The uniform density beam enters the region at $t = 0$ and moves in the z direction at velocity v_i. We resolve the problem of inconsistent boundary conditions by introducing the possibility of low-energy electrons in the propagating beam. These electrons reflect from the moving ion front – Figure 11.4 illustrates the process. If

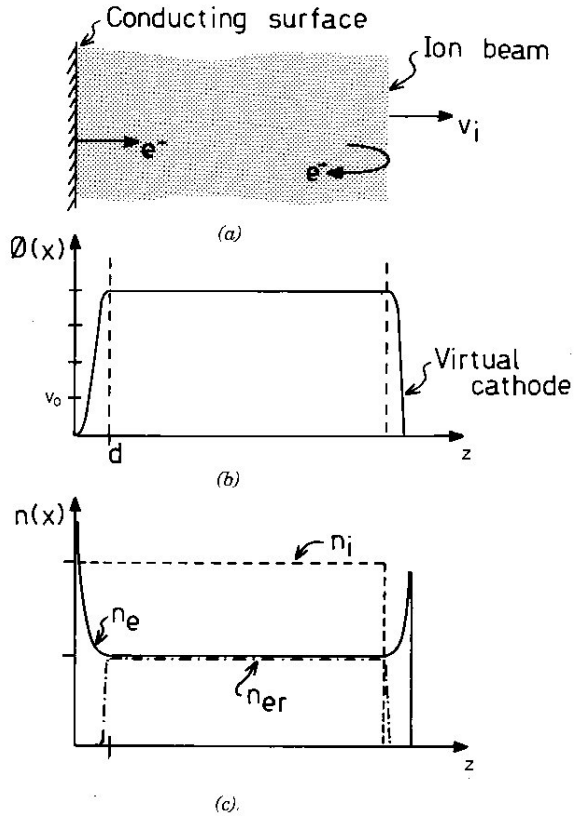

Figure 11.4. Time-dependent solution for ion beam neutralization by the space-charge acceleration of electrons. *a*) Geometry, showing electrons reflected by a virtual cathode at the moving ion front. *b*) Variation of electrostatic potential with z: $e\phi_o = (m_e/m_i)T_i$. *c*) Spatial variation of densities of ions (n_i), entering electrons (n_e) and reflected electrons (n_{er}).

the potential across the sheath exceeds the voltage V_o, electrons enter the beam with velocity higher than v_i. The electrons try to run ahead of the ion front, but the unbalanced space-charge creates a virtual cathode. Electrons reflected from the moving virtual cathode have reduced kinetic energy.

Suppose that the voltage drop across the sheath equals $4V_o$ – electrons enter the beam with velocity $2v_i$. Applying conservation of momentum, we find that an electron loses all its kinetic energy when reflected from the moving beam front. As a result, the electron distribution in the propagating beam has two components: stationary reflected electrons and a uniform density of newly injected electrons moving at $2v_i$. Conservation of flux implies that the moving ion front deposits stationary electrons at the same rate as electrons exit the acceleration sheath. Therefore, the density of stationary electrons n_s equals the density of injected electrons at the sheath exit $n_e(d)$. In a neutralized beam, the densities are:

$$n_s = n_e(d) = n_o/2. \tag{11.11}$$

By including stationary electrons in the beam, we can solve the Poisson equation in the electron acceleration sheath. The following boundary conditions define the solution:

$$1) \quad \phi(0) = 0. \tag{11.12}$$

$$2) \quad \phi(d) = 4V_o. \tag{11.13}$$

$$3) \quad d\phi(0)/dz = 0. \tag{11.14}$$

$$4) \quad d\phi(d)/dz = 0. \tag{11.15}$$

$$5) \quad n_e(d) = n_o/2. \tag{11.16}$$

Equation (11.16) implies that the density of electrons near the exit of the sheath is lower than the ion density. By Eq. (11.5), the electron density is higher near the cathode grid. Therefore, it is possible to generate a solution for ϕ that follows an S-shaped curve. The solution of the Poisson equation with conditions (11.12) through (11.16) is identical to Eq. (11.10) in the sheath region, $0 \le z \le d$. The sheath width is

$$d = \pi\,(2V_o\epsilon_o/en_o)^{1/2}. \tag{11.17}$$

In the region $z > d$ the additional low-energy electrons give a solution with constant potential, $\phi = 4V_o$, rather than the oscillatory solution of Figure 11.3. The electric field is confined to the sheath. The propagating beam is field-free. In the beam volume, the net electron density equals n_o while the *average* electron velocity equals v_i. Figure 11.4 shows a plot of electron density and potential over the sheath and beam.

The modified sheath solution gives an electron distribution in the beam with two discrete velocity components at $v_e = 0$ and $v_e = 2v_i$. In the beam rest frame, the electron components stream through each other with velocity $\pm v_i$. Such a distribution is potentially unstable to the two-stream instability (Section 14.1). This instability randomizes the axial velocity distribution. We can find the actual electron distribution that results from auto-neutralization from a one-dimensional computer simulation. Figure 11.5 shows results from a computer program that uses the dimensionless variables of Eqs. (11.7) and (11.8). The figure gives electron phase-space distributions in terms of the dimensionless electron velocity $V = v_e(z)/v_i$. Figure 11.5*a* shows a distribution at early time when the ion beam has moved only a few sheath widths. The spatial variation of electron velocity closely follows the prediction of Eq. (11.10). As predicted, the peak potential of $4V_o$ occurs at a distance $Z = (2)^{1/2}\pi$ from the source. The solution has an oscillatory component of potential similar to that of Figure 11.3. Some reflected electrons appear as negative velocity particles.

Figure 11.5*b* shows the electron distribution at a later time with the ion beam front at $Z = 9$. There is considerable activity near the injection point, but the downstream electrons have settled into an equilibrium with small variations of potential. The average beam potential is V_o and the average electron velocity equals v_i. Thermalization of the electron distribution results from the

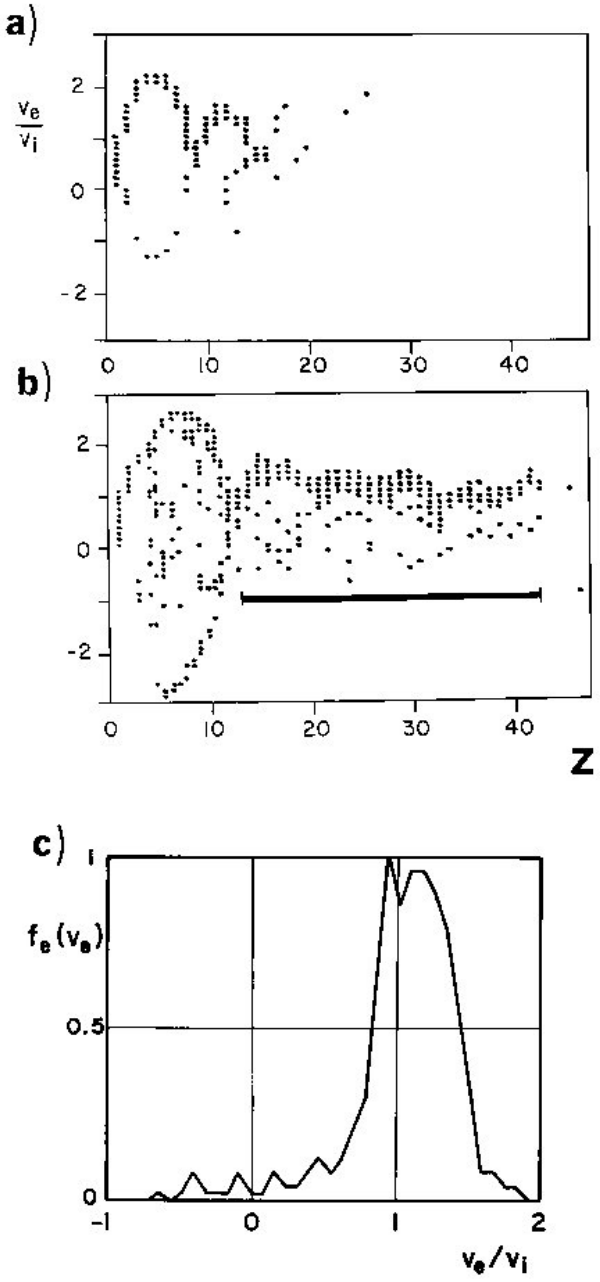

Figure 11.5. Particle-in-cell computer simulation of one-dimensional auto-neutralization. A uniform-density ion beam with a sharp front moves into a field-free region. Ion kinetic energy: T_i, ion velocity: v_i, ion beam density: n_o. $V_o = (m_e/m_i)T_i$, $Z = z/(\epsilon_o V_o/en_o)^{1/2}$. *a*) Axial phase-space plot of the electron distribution with the ion front at $Z = 15$. *b*) Axial phase space plot of the electron distribution with the ion front at $Z = 40$. *c*) Relative electron velocity distribution, averaged over the spatial region marked by the thick line in part (*b*).

two-stream instability. Figure 11.5*c* plots the electron velocity distribution averaged over the downstream region of Figure 11.5*b*. The computer simulation illustrates the main difference between auto-neutralization and ideal active neutralization. For the auto-neutralization solution, the electrons have a velocity spread of about $\Delta v_e = 0.6 v_i$ (full-width at half-maximum).

We can use Eq. (11.17) to find the electron acceleration sheath width. Again, suppose we have a 100 keV deuteron beam with density 10^4 A/m^2 – the predicted sheath width is 1.2 mm. This width is much smaller than the width of a high-current ion beam; therefore, the one-dimensional

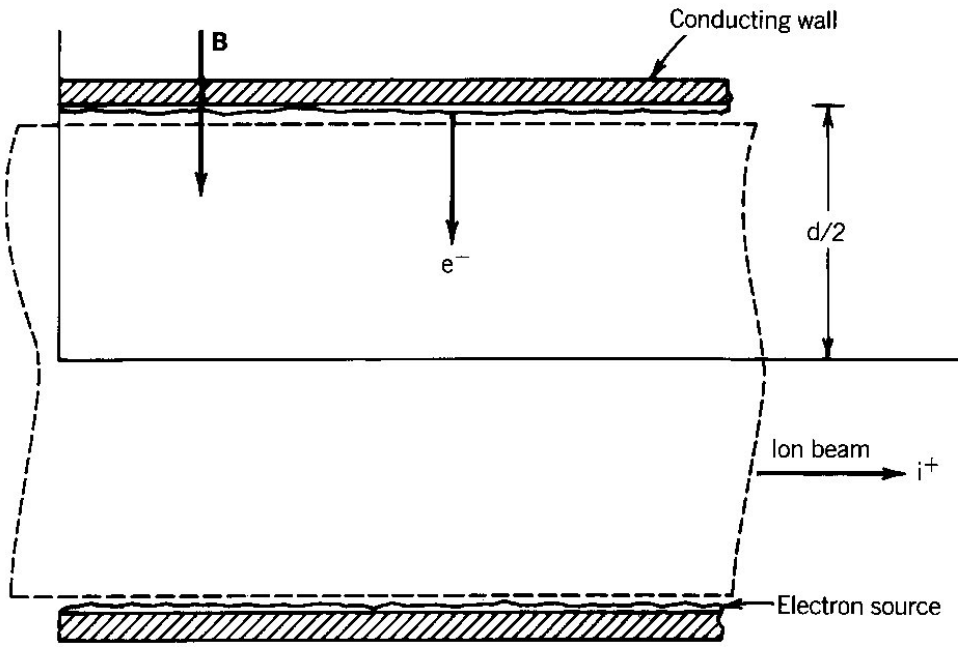

Figure 11.6. Schematic drawing of the transverse neutralization process.

sheath model is a good representation. In many intense ion beam experiments neutralizing electrons are generated when the beam passes through a conducting grid or foil. A localized plasma sheet can also supply electrons for auto-neutralization.

11.2. Transverse neutralization

Figure 11.6 shows the geometry for transverse neutralization of an ion beam. The beam passes between conducting boundaries that act as electron sources. The space-charge electric field of the ions pulls electrons from the boundaries. Ideally, the electrons cancel electric fields in the beam. The main differences from the models of Section 11.1 are that the ions propagate through a bounded region and that the electrons need not move with the ion beam. By studying transverse neutralization, we can understand how electrons merge with ion beams in more complex geometries.

The geometry of Figure 11.6 is a good representation of the transport region near a magnetically-insulated ion diode (Section 8.8). The diode magnetic field penetrates into the transport region, inhibiting axial propagation of neutralizing electrons. The electrons can flow only along the magnetic field lines. In a vacuum, the only way to neutralize an intense ion beam is to supply electrons on all magnetic field lines that the beam crosses. Electrons generated on the surfaces shown in Figure 11.6 flow into the beam. For intense ion beam diodes with pulse lengths less than 0.1 μs, we must study the response time for this process to determine the success of transverse neutralization.

We shall take an approach similar to that of Section 11.1. We start with a simple equilibrium model that has reasonable assumptions but leads to non-physical results. By analyzing the limitations of the model, we can gain insight into how neutralization occurs in a real system. Finally, to get an accurate description of the disordered collective process we turn to computer simulations. For the simplified one-dimensional model, suppose that an ion beam moves in the z direction through a field-free region between two conducting walls at $x = \pm d/2$. The walls can supply a space-charge-limited electron flux. We assume that the maximum space-charge potential energy is much smaller than the ion kinetic energy, $e\phi \ll T_i$. Therefore, we shall concentrate on the electron motion. For simplicity, we let the ions fill the space between the boundaries with a uniform density n_o.

For one-dimensional motion the density of electrons is inversely proportional to their velocity in the x direction. The density is related to the electrostatic potential by

$$n_e = A/\phi^{1/2}. \tag{11.18}$$

We define the wall potential as $\phi(\pm d/2) = 0$. For space-charge-limited electron emission, the wall electric field equals zero, $d\phi(\pm d/2)/dx = 0$. The electric field also equals zero on the symmetry axis, $d\phi(0)/dx = 0$. We can write the Poisson equation for a space-charge equilibrium as:

$$\frac{d^2\phi}{dx^2} = -\frac{e}{\epsilon_o}\left[n_o - \frac{A}{\phi^{1/2}}\right]. \tag{11.19}$$

We define the quantity ϕ_o as the potential at the midpoint between the boundaries, $\phi(0) = \phi_o$. The first integral of Eq. (11.19) is:

$$\frac{d\phi}{dx} = -\frac{2e}{\epsilon_o}\left[n_o\phi - n_o\phi_o - 2A\phi^{1/2} + 2A\phi_o^{1/2}\right]. \tag{11.20}$$

Equation (11.20) satisfies the boundary conditions if $A = n_o\phi_o^{1/2}/2$. Substituting for A and introducing dimensionless variables $\Phi = \phi/\phi_o$, $X = x/x_o$, Eq. (11.20) becomes:

$$\int_1^{\Phi} \frac{d\Phi'}{(\Phi^{1/2} - \Phi')^{1/2}} = \pm\left[\frac{2en_od^2}{\epsilon_o\phi_o}\right]^{1/2} X. \tag{11.21}$$

Equation (11.21) has the multiple solutions:

$$\pm X = \left[\frac{2\pi\epsilon_o\phi_o}{en_od^2}\right]^{1/2}\left[2(\Phi^{1/2} - \Phi)^{1/2} - \sin^{-1}(2\Phi^{1/2} - 1) + \sin^{-1}(1)\right]. \tag{11.22}$$

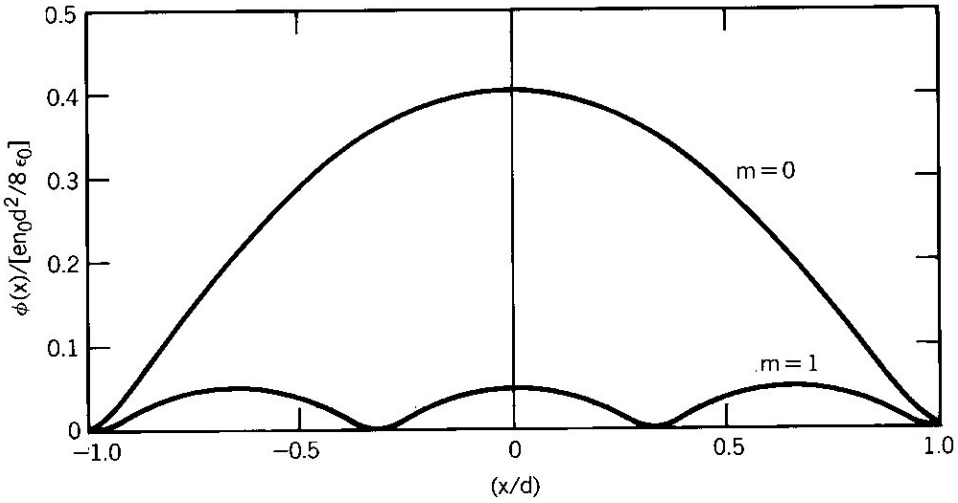

Figure 11.7. Spatial variations of electrostatic potential for transverse neutralization with ideal one-dimensional electron motion and an ion density constant over all time.

The maximum electrostatic potential, $\Phi = 1$, occurs at the midplane $X = 0$. In physical units, the midplane potential is:

$$\phi_o = en_o d^2/2\pi^2\epsilon_o(2m+1)^2. \tag{11.23}$$

where $m = 0,1,2,....$ The maximum potential from a uniform-density ion beam without neutralizing electrons is $en_o d^2/8\epsilon_o$. We define a space-charge potential reduction factor:

$$\phi_o/[en_o d^2/8\epsilon_o] = 4/\pi^2(2m+1)^2. \tag{11.24}$$

Figure 11.7 shows the spatial variation of potential of neutralized and unneutralized beams for different values of m.

One problem with the model is that it does not predict a unique equilibrium state. We expect that a unique set of initial conditions should give a unique final state. We can choose any value of m – the model does not show whether neutralization is effective. For $m = 0$ the reduction factor equals 0.405. This reduction is useless for intense ion beam transport where the electric fields must be less than a factor of 10^{-6} of the unneutralized value.

The simplified model is unrealistic for two reasons. First, it takes electron motion as perfectly one-dimensional. In consequence conservation of energy implies that an electron that leaves one boundary reaches the other boundary with zero velocity. Therefore the density of reflexing electrons diverges at the boundaries. For the $m = 0$ solution electrons spend most of the time near the boundaries and move quickly through the midplane. As a result the ion beam is over-neutralized at the boundary and under-neutralized at the midplane. Another problem with the

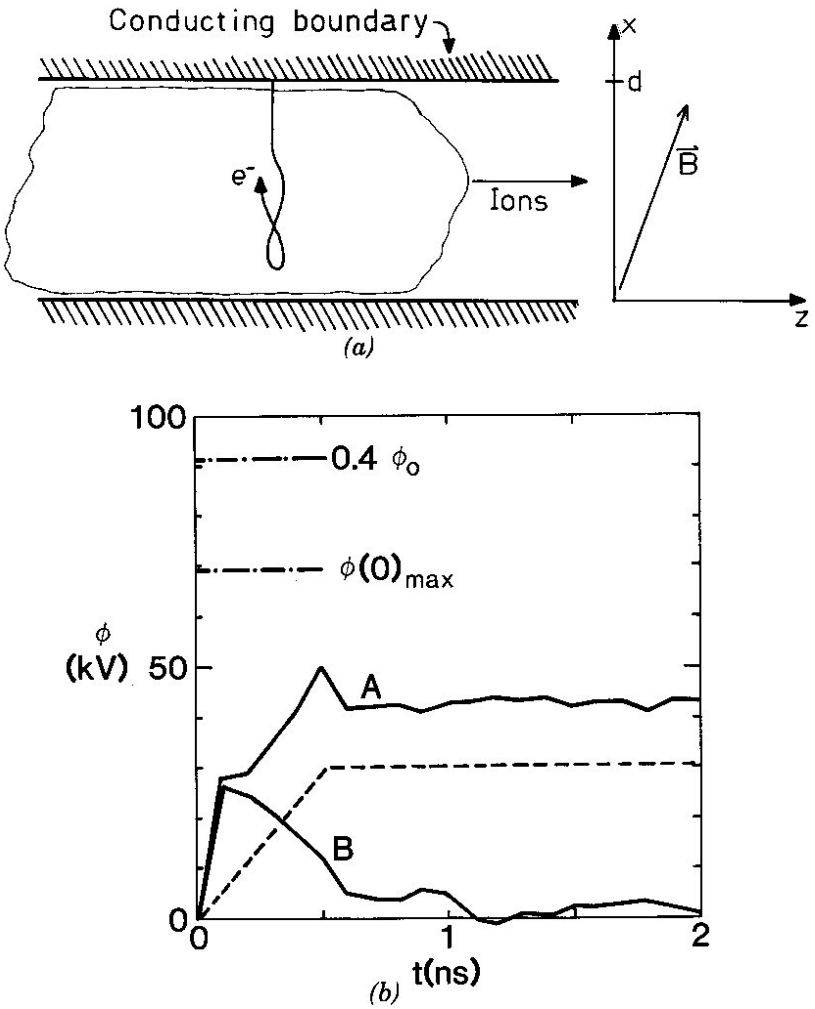

Figure 11.8. Particle-in-cell computer simulation of transverse neutralization. *a*) Simulation geometry – the ion density increases with time between grounded conducting electron emitters. The figure shows an electron orbit deflected by a skewed magnetic field. *b*) Simulation results - time-variation of electrostatic potential on the midplane. Dashed line shows variation of ion density with peak value $n_o = 10^{18}$ m^{-3}. Quantities $0.4\phi_o$ and $\phi(0)_{max}$ described in text. Curve *A*: magnetic field inclination angle: 0° - one-dimensional electron motion. Curve *B*: magnetic field inclination angle: 15°. (Courtesy, J. Poukey, Sandia National Laboratories).

model is that the monoenergetic electron distribution is valid only if the ion density is constant at all times. For a pulsed beam the ion density and the associated space-charge fields change with time. Therefore, electrons emitted early in the pulse have different orbit properties than those that enter at late times.

Transverse neutralization is effective if electrons in the beam volume do not return to the boundary. If electrons are trapped in the beam volume, then additional electrons can enter from the boundaries until space-charge fields are completely canceled. Relaxing the constraint of one-dimensional motion allows electron trapping. If an electron suffers a deflection normal to the x direction (Figure 11.8*a*), conservation of energy implies that it cannot return to the boundaries. A temporal variation of space-charge fields also traps electrons. A rising ion density pulls electrons away from the boundary.

A computer simulation is the best approach to model complex electron orbits. We shall review results from a particle-in-cell simulation for the geometry of Figure 11.8*a*. Electrons leave conducting boundaries with a space-charge-limited flux. The boundaries and ion density have infinite extent in the z direction. The ion density is also uniform in the x direction. The simulation model has two main differences from the simple equilibrium model:

1) The ion density rises with time to an equilibrium value.

2) A transverse magnetic field in the transport region influences the electron orbits. When the magnetic field points along x the electrons have purely one-dimensional orbits as before. On the other hand, tipping the field direction (Figure 11.8*a*) results in electron velocity components in the y and z directions.

The skewed magnetic field is an easy way to introduce the effect of geometric variations into the one-dimensional code.

Figure 11.8*b* shows results of the simulation. The graph plots the electrostatic potential at the midplane ϕ_o as a function of time. The boundaries are at positions $d = \pm 0.005$ m, the ion density rises to a final value $n_o = 10^{18}$ m^{-3} with a rise time $\Delta t_r = 0.5$ ns. The dashed line in Figure 11.8*b* shows the variation of ion density. For the given parameters, the equilibrium model predicts a potential $\phi_o = [0.405 e n_o d^2/8\epsilon_o] = 91$ kV for $m = 0$. Curve *A* of the figure corresponds to a calculation where the magnetic field lies in the x direction. The reduced potential results from the time dependence of space-charge fields. The final potential is lower than the equilibrium model prediction by about a factor of two. Curve *B* is the result of a simulation with deflected electron orbits – the magnetic field has an inclination of 15°. This small change in geometry results in a dramatic difference in the nature of the solution. After the ion density reaches equilibrium, the potential rapidly drops almost to zero. (The residual potential oscillations at late time result from the finite number of particles in the simulation.) The simulation implies that in real systems with asymmetries, transverse electron neutralization rapidly cancels space-charge electric fields.

Because of their low mass, electrons respond rapidly to changes in the density of an ion beam. Nonetheless, the variation of ion density in pulsed ion diodes is so rapid that the electron response time can result in high values of space-charge potential. The simulation results (Figure 11.8*b*) show that a non-zero space-charge potential is necessary to draw electrons into the beam volume during the rise of ion density. We can estimate the required potential for the geometry of Figure 11.9. A sheet ion beam of width $\pm x_b$ and velocity v_i enters a region between electron-emitting plates separated by distance $\pm d$. At a given axial location, the ion density varies as:

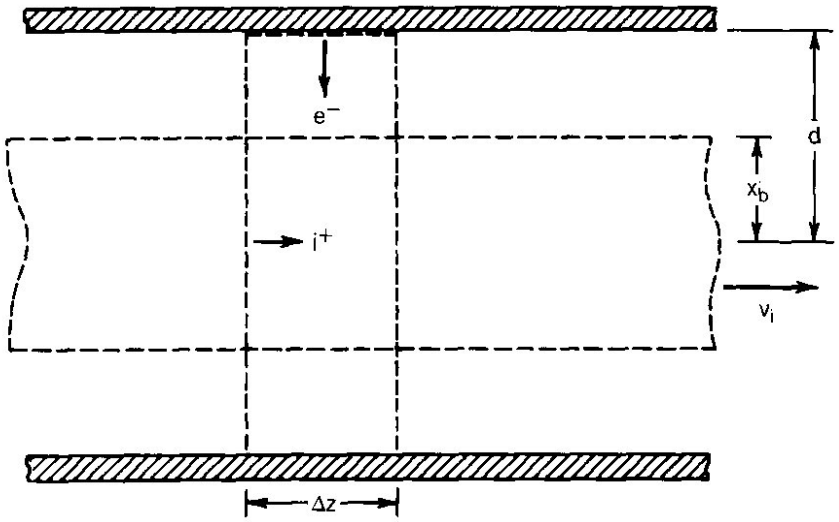

Figure 11.9. Geometry to estimate the peak electrostatic potential in an ion beam with rising density neutralized by the transverse flow of electrons.

$$n_i(t) = n_o(t/\Delta t_r), \tag{11.25}$$

for $t \le \Delta t_r$, and $n_i(t) = n_o$ for $t > \Delta t_r$. When $v_i \Delta t_r \gg d$ the space-charge electric fields lie predominantly in the x direction.

A transverse magnetic field prevents electron motion in the z direction. We can estimate the electrostatic potential during the ion density rise by invoking global charge balance in a section of the transport system of length Δz. During the rise of ion density, the beam potential must be high enough to pull electrons across the vacuum region from the walls. We assume that field asymmetries are strong enough to trap electrons in the beam; therefore, electrons enter continually from the wall. Finally, we assume that neutralization is effective so that the global integrals of electron and ion densities over the volume element $2d\Delta z\Delta y$ are almost equal, or

$$\Delta z \Delta y \int_{-d}^{+d} dx \, \frac{\partial n_i}{\partial t} \cong \Delta z \Delta y \int_{-d}^{+d} dx \, \frac{\partial n_e}{\partial t} \, . \tag{11.26}$$

Equation (11.26) holds when the space-charge potential is much smaller than that of an unneutralized beam.

The integral of the time variation of ion density over the volume element of Fig. 11.9 equals:

$$\Delta z \Delta y \int_{-d}^{+d} dx \, \frac{\partial n_i}{\partial t} \cong (2x_b \, \Delta z \Delta y) \, n_o \, / \Delta t_r \, . \tag{11.27}$$

If the current density of electrons leaving each boundary is j_e and if the beam traps the electrons, the rate of change of the integrated electron density is approximately:

$$\Delta z \Delta y \int_{-d}^{+d} dx \, \frac{\partial n_e}{\partial t} \cong 2 \left(\frac{j_e}{e} \right) \Delta z \Delta y \ . \tag{11.28}$$

If ϕ_o represents the average electrostatic potential of the beam, the electron current density scales as:

$$j_e \leq (4\epsilon_o/9) \, (2e/m_e)^{1/2} \, \phi_o^{3/2}/d^2. \tag{11.29}$$

The inequality depends on the fraction of the transport region filled by the ion beam. Combining Eqs. (11.26) through (11.29) gives the following expression for the beam potential during the ion density rise:

$$\phi_o \leq \left[\frac{9}{8} \, \frac{en_o}{\epsilon_o \Delta t_r} \, d^2 x_b \left(\frac{m_e}{2e} \right)^{1/2} \right] . \tag{11.30}$$

When applied to the parameters of the simulation of Figure 11.8 (where the ion beam fills the transport region), Eq. (11.30) overestimates the potential by about a factor of 2.5. The dashed line in the figure shows the estimate. As an application example consider a neutralized ion beam accelerator (Section 11.5). A Na^+ beam has current density 50×10^4 A/m^2, kinetic energy 20 MeV, and ion density $n_o = 2.4 \times 10^{17}$ m^{-3}. The beam has width $x_b = 0.02$ m and propagates between boundaries at d = ·0.04 m. With a beam density risetime of 50 ns, the predicted midplane electrostatic potential is $\phi_o \leq 30$ kV. The transverse electric fields associated with the residual potential can result in beam defocusing, limiting the utility of high-current ion diodes and accelerators.

11.3. Current neutralization under vacuum

When a high-current ion beam moves into an infinite field-free volume, accompanying electrons provide both space-charge neutralization and current neutralization. We can show that a high-flux ion beam is also current-neutralized if it crosses a finite length region from a source to an electrically-isolated target. Without electron flow, the beam would induce a large voltage drop between the target and source. As an example, suppose a focused ion beam charges a spherical target of radius 0.1 m. The beam has 10 A current and a 1 MeV kinetic energy. If the distance between target and the source is 0.3 m, the inter-electrode capacitance is about $C = 10^{-12}$ F. The voltage difference is $\Delta V \cong I_i \Delta t / C$, where Δt is the beam pulse length. The deposited

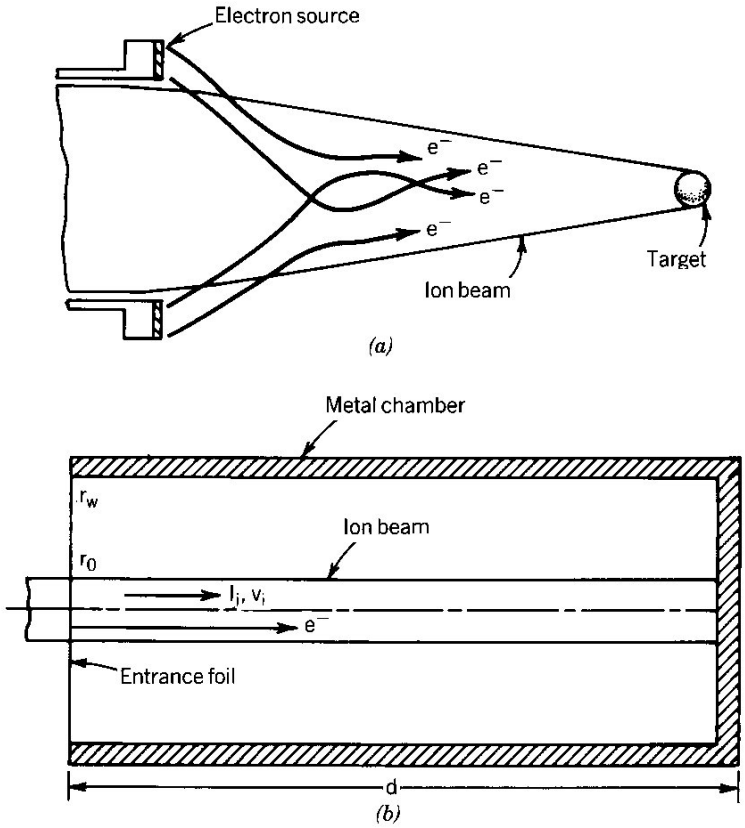

Figure 11.10. Current neutralization of ion beams by electron flow in vacuum. *a*) Intense ion beam focused to an inertial fusion target. *b*) Ion beam in a closed pipe neutralized by the axial flow of electrons.

charge creates a potential equal to the beam kinetic energy in about 1 μs. On the other hand, the voltage to accelerate an equal current of electrons is only about 500 V. We expect that if electrons are available at the source electrode, they will flow to the target with the ion beam to cancel the space-charge potential. Figure 11.10*a* shows the elements of a one-dimensional auto-neutralization solution for an ion beam crossing to an isolated target. The net current to the target is zero if it has potential is $+eV_o$.

The current of an intense ion beam is not canceled completely when the beam moves through a vacuum region surrounded by conducting boundaries. To describe time variations of the electron current, we shall use the idealized geometry of Figure 11.10*b*. A cylindrical beam of ions with kinetic energy T_i travels through a pipe of radius r_w and length d with conducting walls at each end. The beam has current I_i, radius r_o and velocity $v_i \cong (2T_i/m_i)^{1/2}$. The source plane can supply an electron flux equal to the beam current density. For current neutralization, the electrons must have kinetic energy; on the other hand, stationary electrons could provide space-charge neutralization. In the static field limit there are no electric fields to give electrons a directed energy because the surrounding walls are all grounded. At late time (compared with the ion

transit time d/v_i), we expect that the neutralizing electrons are stationary. Inside the pipe there are no electric fields but there are magnetic fields created by the ion beam current.

Processes are more interesting at early times because the changing magnetic flux inside the pipe can create an axial electric field to accelerate neutralizing electrons. During the initial transit of the beam front through the pipe, electrons follow the beam with velocity v_i. In this phase, the electron distribution is determined by the auto-neutralization process described in Section 11.2. When the beam contacts the downstream wall the flow of neutralizing electrons continues. If the electron flow were to stop immediately, the toroidal magnetic field of the beam would appear instantaneously, creating an infinite electric field. Therefore, the electron flow must decrease gradually. For current neutralization to persist, a continuous flow of electrons from the entrance wall must accelerate to kinetic energy $T_{eo} = (m_e/m_i)T_i$. Changing magnetic flux inside the pipe supplies the accelerating voltage. The small fractional deceleration of ions in the electron acceleration sheath at the entrance wall contributes energy to create the magnetic field. The inductive voltage results from a changing net current. Because the ion current density is constant the electron current must decay.

We can construct a simple model for the decay of neutralizing electron current with the following assumptions:

1. The ion beam current rises rapidly. During the initial ion transit through the pipe, the electron current equals the ion current. At time $t = 0$ when the beam fills the pipe, the net current equals zero. If $I_e(t)$ is the net electron current, then $I_e(0) = -I_i$.

2. Electrons accelerate in a narrow sheath at the entrance wall. We denote the average electron kinetic energy at $t = 0$ as $T_e(0) = T_{eo}$.

3. The beam radius is much smaller than the pipe radius, $r_o \ll r_w$. As a result, the magnetic field energy from a net chamber current is concentrated in the volume outside the beam. To first order, the inductive voltage acts uniformly on all electrons.

4. The ion and electron densities n_i and n_e are uniform over the beam radius.

5. The space-charge of the high-intensity ion beam is always neutralized. Thus, the electron density always equals the ion density, $n_e \cong n_i$.

The ion current I_i is constant following injection, while the magnitude of the electron current $I_e(t)$ decreases in time. The net current is $I(t) = I_i - I_e(t)$. The chamber has an inductance L roughly equal to:

$$L = (\mu_o/2\pi)\, d\, \ln(r_w/r_o). \tag{11.31}$$

The voltage between the entrance and exit walls is:

$$V = L\, (dI/dt). \tag{11.32}$$

Because the electron and ion densities are always equal, the ratio of ion to electron current is proportional to the ratio of the average particle velocities:

$$I_e/I_i = v_e/v_i. \tag{11.33}$$

where $v_e(t) = (2T_e(t)/m_e)^{1/2}$. We can rewrite Eq. (11.33) as:

$$I = I_i\ (1 - v_e/v_i). \tag{11.34}$$

The electrons gain their velocity in a narrow sheath at the entrance wall. With this condition, Eq. (11.34) becomes

$$I = I_i\ (1 - \sqrt{eV/T_e})\ . \tag{11.35}$$

We can combine Eqs. (11.32) and (11.35) into a single equation for the time-variation of total current:

$$L\ (dI/dt) = (T_{eo}/e)[1 - (I/I_i)]^2. \tag{11.36}$$

In terms of the dimensionless variables,

$$\tau = t/(eLI_i/T_{eo}), \tag{11.37}$$

and

$$\mathrm{I} = I/I_i, \tag{11.38}$$

Equation (11.36) becomes:

$$d\mathrm{I}/d\tau = (1 - \mathrm{I})^2. \tag{11.39}$$

With the initial condition that $\mathrm{I} = 0$ at $\tau = 0$, the solution of Eq. (11.39) is:

$$\frac{\mathrm{I}}{\mathrm{I}_i} = 1 - \frac{1}{1+\tau}\ . \tag{11.40}$$

Figure 11.11 plots the result of Eq. (11.40). The net current rises to a significant level over the dimensionless interval $\tau = 1$. At late time the total current approaches the ion current. As expected, stationary electrons provide long-term space-charge neutralization.

In most experiments with pulsed high-current ion beams in bounded chambers the fractional decay of electron current is small. For example, suppose we have a high-flux beam of 500 keV

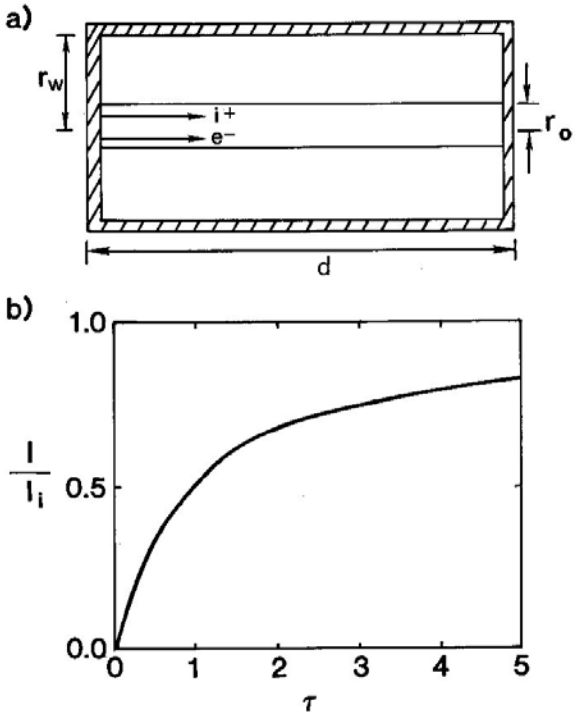

Figure 11.11. Variation of the net current for a neutralized ion beam inside a closed pipe. *a*) Geometry of the calculation. b) Variation of total current I as a function of time. I_i equals the constant injected ion current, τ equals $t/(eLI_i/T_{eo})$, and L equals $(\mu_o/2\pi)d\ \ln(r_w/r_o)$.

protons with $j_i = 100 \times 10^4$ A/m^2, and $r_o = 0.05$ m. The beam travels through a drift chamber of length $d = 1$ m and radius $r_w = 0.15$ m. The total beam current is $I_i = 7.9$ kA, the chamber inductance is $L \cong 2.2 \times 10^{-7}$ H, and the average electron energy for current neutralization is $T_{eo} =$ 271 eV. Inserting the values in Eq. (11.37), the characteristic current decay time is $\tau = LI_ie/T_{eo} =$ 6.4 μs. The quantity τ is much longer than pulselengths typical of many experiments ($\lesssim$0.1 μs).

By adjusting the propagation chamber inductance and the beam width, we can achieve conditions where τ is much shorter than the beam pulselength. In this limit we can use small propagation chambers for measurements of the current density of energetic, neutralized ion beams. Figure 11.12 shows the geometry of a detector. It consists of a bounded cylindrical chamber with a Rogowski loop [CPA, Section 9.14] to measure the net axial current. Ions enter through a foil with thickness less than the ion range. Besides acting as an electron source, the foil provides discrimination against low-energy ions. Each ion in the beam creates several secondary electrons on the inner surface of the foil. We can design the chamber geometry for a rapid decay of electron current. For example, with $d = 0.01$ m, $r_o = 0.002$ m and $r_w = 0.015$ m, the chamber inductance is only $L = 4 \times 10^{-9}$ H. For a beam of 500 keV protons with $j_i = 100 \times 10^4$ A/m^2, the decay time is $\tau = LI_ie/T_e \cong 0.2$ ns. As a result, the detector has good time resolution. We can find the ion current density by dividing the net chamber current by the area of the entranced aperture.

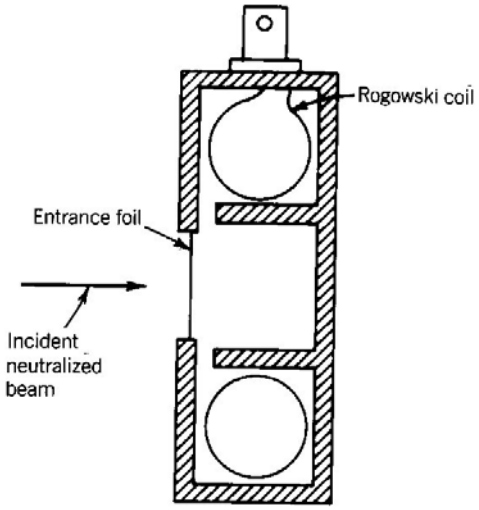

Figure 11.12. A detector to measure the current density of an energetic, high-current ion beam neutralized by electrons. (Courtesy, J. Greenly, Cornell University).

11.4. Focal limits for neutralized ion beams

One motivation to neutralize an ion beam is to focus it to a small spot size. Recent neutralization studies have concentrated on intense ion beam transport to small inertial fusion targets. In Section 5.4, we saw that space-charge forces interfere with focusing. In this section, we shall study processes that limit focusing of neutralized beams in vacuum. Although the focal spot size for a neutralized beam is smaller than that for a bare beam, we shall see that collective effects may present limitations for some applications.

Figure 11.13 shows a pulsed neutralized beam crossing a vacuum region to a target. A current of electrons equal to the ion current enters the beam at the entrance. The electrons almost eliminate electric fields in the beam. Nonetheless, there is a small transverse electric field if the electrons have non-zero transverse temperature, kT_e. Sections 11.1 and 11.2 showed that both the longitudinal and transverse neutralization processes lead to thermal electron distributions. As a first step in the calculation of ion trajectories in a neutralized beam, we shall estimated the magnitude of the thermally-generated fields.

We take an ion beam with cylindrical symmetry — changes in the beam dimension take place over axial distances much larger than the beam radius. The radial variation of high-energy ions is a given function:

$$n_i(r) = n_{io} f(r). \tag{11.41}$$

The quantity n_{io} is the ion density on axis and $f(r)$ is a normalized function that equals unity at $r = 0$ and drops to zero at large radius. We assume that the electron transverse velocity distribution

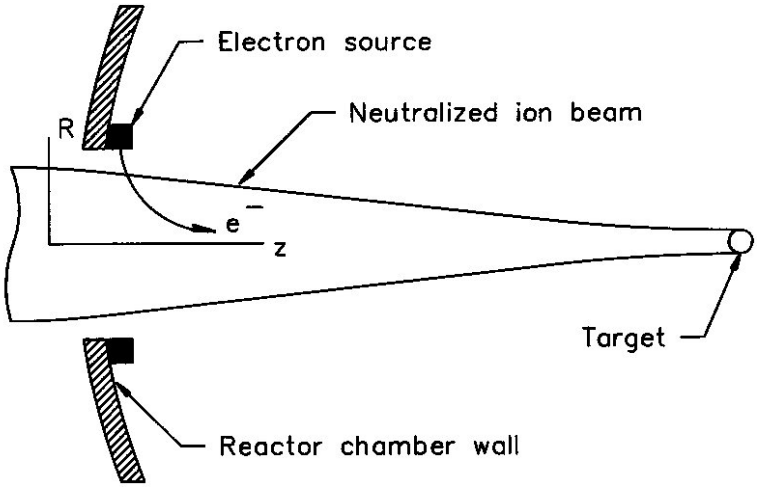

Figure 11.13. Coordinate system to analyze propagation of a pulsed neutralized ion beam to an inertial fusion target in a spherical reactor.

viewed in the beam rest frame is close to a Maxwell distribution with uniform temperature kT_e. Section 2.11 showed that the electron density is related to the electrostatic potential by:

$$n_e(r) = n_{eo} \exp[e\phi(r)/kT_e]. \tag{11.42}$$

With the choice $\phi(0) = 0$, the quantity n_{eo} is the electron density on axis. Although Eq. (11.42) applies only to beams in equilibrium, it is useful to estimate the electron density when the ion beam changes slowly compared with the average electron transit time over the beam-width.

When a neutralized ion beam propagates in free space, the net beam current is zero. The line charges of ions and electron have equal magnitude, or:

$$\int_0^\infty 2\pi r\, dr\, n_i(r) = \int_0^\infty 2\pi r\, dr\, n_e(r)\ . \tag{11.43}$$

When the neutralizing electrons are cold the radial distributions of electrons and ions are identical. On the other hand the density profile of hot electrons may extend radially outside the ion distribution. We can calculate the variation of electron density by substituting Eqs. (11.41) and (11.42) in the cylindrical Poisson equation:

$$\frac{1}{r}\frac{d}{dr}\left(r\frac{d\phi}{dr}\right) = \frac{e}{\epsilon_o}\left[-n_{io}\, f(r) + n_{eo}\exp\left(\frac{e\phi}{kT_e}\right)\right]. \tag{11.44}$$

We can identify the scaling parameters by rewriting Eq. (11.44) in terms of the following dimensionless variables:

$$\Phi = e\phi/kT_e, \tag{11.45}$$

$$R = r/(kT_e\epsilon_o/e^2 n_{eo})^{1/2} = r/\lambda_d, \tag{11.46}$$

where λ_d is the Debye length [Eq. (6.13)]. The reduced form of Eq. (11.44) is:

$$\frac{1}{R}\frac{d}{dR}\left(R\frac{d\Phi}{dR}\right) = \exp(\Phi) - N_{i_o} f(R)\ ,$$

where $N_{io} = n_{io}/n_{eo}$. Inspection of Eq. (11.47) shows that Φ changes significantly over a scale length $R \sim 1$.

We can solve Eq. (11.47) numerically by an integration from the axis to large radius. We initiate the calculation with the starting conditions $\Phi(0) = 0$, $d\Phi(0)/dR = 0$ and an assumed value of N_{io}. Equation (11.43) and Gauss's law imply that the radial electric field outside the beam equals zero. If the choice of N_{io} is correct, $d\Phi/dR$ approaches 0 at infinite radius. Figure 11.14 illustrates two solutions. In the first (Figure 11.14*a*), the ion density is uniform between the axis and a sharp edge. In the second solution (Figure 11.14*b*), the ion density drops smoothly to zero. In both case the transverse temperature pushes electrons outside the ion distribution. The ion density exceeds the electron density near the axis. As a result, there is a positive radial electric field. The equilibrium solution represents a balance between the radial electric force and the gradient of the electron pressure.

For an ion beam with a well-defined boundary, the electric field is concentrated within a few Debye lengths of the edge. The peak electric field roughly equals:

$$E_r \sim kT_e/\lambda_d e. \tag{11.48}$$

For the smooth beam profile, charge separation occurs over the fill width of the beam. The radial variation of electric field is almost linear.

We can use Eq. (11.48) to estimate the effects of electron temperature on neutralized ion beam focusing. Figure 11.13 shows the geometry of the calculation. Ions enter a spherical chamber and travel through vacuum to a small target. At the entrance point, the ions draw electrons from a source. Following Section 11.1 we expect that the entering electrons have a small but non-zero temperature kT_{eo}. Near the entrance, electric fields resulting from electron temperature are small and have a negligible effect on the ion orbits. On the other hand electric fields resulting from electron temperature can be very strong near the target. In a short neutralized ion beam the

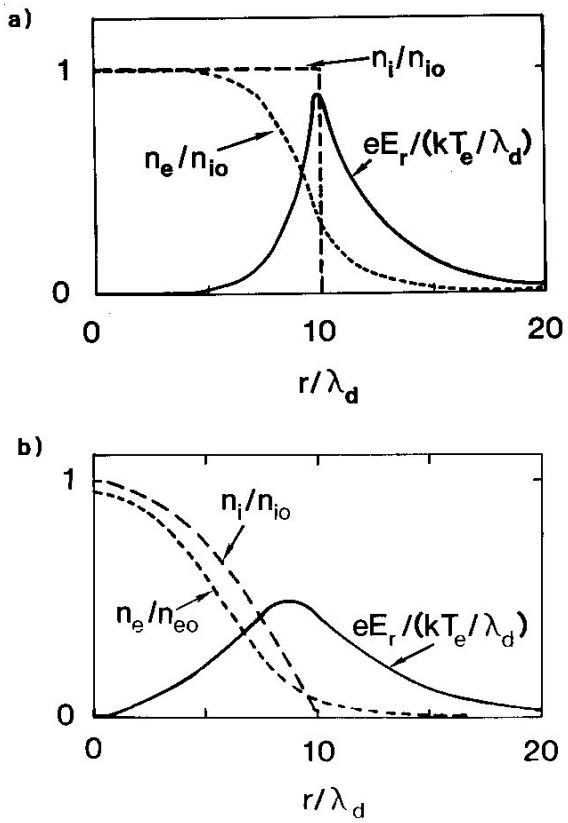

Figure 11.14. Spatial variations of normalized particle density and radial electric field for a cylindrical ion beam neutralized by hot electrons with temperature T_e. $\lambda_d = (kT_e\epsilon_o/e^2n_{eo})^{1/2}$. *a*) Uniform density ion beam with a sharp boundary. *b*) Ion beam with a gradual density decrease to zero.

volume occupied by electrons shrinks substantially as the beam moves toward a focus. Compression of the electrons raises their temperature.

We shall use an envelope equation to describe propagation of a neutralized ion beam. The process of neutralized beam focusing is complex – our model illustrates the application of approximations and the limitations they introduce. The main assumption is that the length of the ion beam pulse is much shorter than the distance from the injection point to the target. As a result, the ions and electrons form a closed system during propagation. Given the initial electron distribution we can estimate the final properties by applying the principle of phase volume conservation (Section 3.8). If the beam is not isolated, an exchange of hot electrons in the beam for cold electrons from the vacuum chamber or target can take place. This process is much more involved so that we must turn to computer simulations for predictions.

We take the electron distribution at injection as isotropic with temperature kT_{eo}. As the beam travels to the focal point, the electrons compress radially. As a result, the electron temperature varies with the axial position of the beam, $T_e(z) \geq T_{eo}$. We can describe the compression of electrons in two special cases:

1) For an ideal radial compression, the transverse energy of electrons increases while the thermal energy in the axial direction remains constant. We apply the theory of Section 3.8 for a two-dimensional compression.

2) If the beam compression is non-uniform in the z direction, some of the transverse energy gain converts to an axial velocity spread. If there is strong coupling between axial and transverse motion, the electron velocity distribution remains isotropic. Here, the beam undergoes a two-dimensional compression with energy shared between three degrees of freedom.

The final electron distribution of a real beam is likely to have properties intermediate between the predictions of the two limiting cases.

The solutions of Eq. (11.47) imply that the radial electric field at the beam roughly equals:

$$E_r(z) \cong \eta\, (kT_e(z)/e\lambda_d). \tag{11.49}$$

The quantity $T_e(z)$ is the transverse electron temperature and η is a scaling parameter with a value near 0.5. The Debye length of electrons in the beam changes with propagation distance according to

$$\lambda_d(z) = \lambda_{do} \left[\frac{kT_e(z)}{kT_{eo}}\right]^{1/2} \left[\frac{n_{eo}}{n(z)}\right]^{1/2}. \tag{11.50}$$

For a radial compression, the electron density is related to the envelope radius R by

$$n_e(z) = n_{eo}\, [R_o/R(z)]^{1/2}. \tag{11.51}$$

To construct an envelope equation, we need an expression for the transverse temperature as a function of the beam radius. To begin, consider an ideal two-dimensional compression. From Section 3.8,

$$kT_e(z) = kT_{eo}\, (R_o/R)^2. \tag{11.52}$$

Substitution of Eq. (11.52) in (11.50) shows that the Debye length is constant during propagation, $\lambda_d(z) = \lambda_{do}$. For the parameters of inertial fusion beams, the Debye length near the focal point often exceeds the beam radius. Therefore, the radial electric fields are close to those of an unneutralized beam near the target.

Combining Eqs. (11.49), (11.50), (11.51) and (11.52) leads to the following expression for the envelope electric field as a function of radius:

$$E_r(R) \cong (\eta kT_{eo}/e\lambda_{do})\, (R_o/R)^2. \tag{11.53}$$

The envelope equation for a nonrelativistic ion beam with zero emittance in a field-free region is

$$R'' = [\eta k T_{eo} R_o^2 / m_i v_i^2 \lambda_{do}]/R^2. \tag{11.54}$$

We can integrate Eq. (11.54) from the target at $z = 0$ back to the injection point at $z = -L$. Assume that the beam has a waist at the target so that $R(0) = R_{min}$ and $R'(0) = 0$. At the injection point $R(-L) = R_o$ and $R'(-\mathbf{L}) = -\theta_o$. The quantity θ_o is the envelope injection angle, $\theta_o \cong R_o/L$. We find that:

$$[R'(z)]^2 = \left(\frac{2\eta \ kT_{eo} \ R_o}{m_i v_i^2 \ \lambda_{do}} \right) \left[\frac{1}{R_{min}} - \frac{1}{R(z)} \right]. \tag{11.55}$$

The quantity v_i is the axial ion velocity. If we drop the term $1/R(z)$ in brackets, Eq. (11.55) leads to a relationship for the minimum beam spot size:

$$\frac{R_{min}}{R_o} \cong \left[\frac{\eta k T_{eo}}{T_i} \right] \left[\frac{R_o}{\lambda_{do}} \right] \left[\frac{L}{R_o} \right]^2. \tag{11.56}$$

The quantity T_i is the ion kinetic energy $m_i v_i^2/2$.

We find a different result from Eq. (11.56) if the electron energy growth is uniform in three dimensions. Conservation of phase volume (Section 3.8) implies that:

$$kT_e(z) = kT_{eo} (R_o/R)^{4/3}. \tag{11.57}$$

Using Eq. (11.57) in place of Eq. (11.52), the predicted focal spot size is:

$$\frac{R_{min}}{R_o} \cong \left[\frac{3\eta \ kT_{eo} \ L^2}{2T_i \ R_o \ \lambda_{do}} \right]^{3/2}. \tag{11.58}$$

We can illustrate the implications of Eqs. (11.56) and (11.58) for beam parameters in a conceptual heavy ion fusion reactor. Suppose that multiple beams of 10 GeV U^+ ions irradiate a target. Each beam radius is $R_o = 0.06$ m while the propagation distance is $L = 10$ m. The beam length of 0.9 m is shorter than the propagation length. Neutralizing electrons with the same velocity as the ions have a kinetic energy of 23 keV. Following the discussion of Section 11.1 we assume an initial electron temperature of $kT_{eo} \cong 10$ keV. The initial density of ions and neutralizing electrons is $n_{eo} = 3.1 \times 10^{16}$ m^{-3}. The initial Debye length, $\lambda_{do} \cong 4.2$ mm, is much smaller than the beam radius. Inserting the parameters into Eq. (11.56) with $\eta = 0.5$ gives a spot size prediction of $R_{min} = 12$ mm for an ideal two-dimensional compression. If the thermal energy is equal in three dimensions, the spot size from Eq. (11.58) is $R_{min} = 5.3$ mm. In both cases the predicted radius is larger than a fusion target. Therefore, the problem of thermally-generated

electric fields warrants detailed study. Our simplified model may over-estimate the electric fields near the target. When the beam contacts the target, hot electrons may exchange with cold electrons from the target surface, short-circuiting the transverse electric fields.

11.5. Acceleration and transport of neutralized ion beams

Neutralized ion beams can carry high power densities – beam currents may exceed 1 kA. Such beams present special problems for acceleration and transport. It is essential to maintain a close balance between ion and electron density throughout the acceleration process. In this section we shall discuss methods to guide neutralized beams and to increase their kinetic energy. Conventional methods of beam focusing, such as electrostatic lenses or quadrupole magnets, are ineffective. The fields in these devices strongly deflect electrons and may interfere with neutralization of the ion beam. Here, we shall concentrate on alternative focusing methods based on collective effects. High-density ion beams cannot propagate without neutralizing electrons. By inducing small electron displacements we can generate large space-charge electric fields that can guide energetic ions.

Figure 11.15*a* shows a simple example of electron control for a high-intensity ion beam. A neutralized beam enters a vacuum region through a grounded grid. The entering ion and electron fluxes are exactly equal. The ion beam has non-zero emittance – we represent the spread in velocity by a transverse temperature kT_i. The region has an applied solenoidal magnetic field B_o. Although the field is too weak to affect the orbits of energetic ions directly, it is strong enough to confine the low-energy neutralizing electrons. In the propagation region the ions expand while the electrons are confined to a cylindrical volume. The resulting charge separation creates radial electric fields that can focus the ions.

Exact solutions for the electrostatic potential in the electrostatic sheath at the edge of the beam depend on details of the ion distribution. Here we shall make a rough estimate of the sheath dimension from scaling arguments. A strong magnetic field bonds electrons to field lines. In the strong field limit electrostatic effects determine the sheath width. If the ions have a Maxwell distribution in transverse velocity, we can apply the results of Section 6.2 to find the sheath width. The width is close to an ion Debye length:

$$\lambda_E \sim (kT_i \epsilon_o / e^2 n_i)^{1/2} . \tag{11.59}$$

In Equation (11.59) n_i is the density of the entering ion beam and the subscript E denotes the sheath width from electrostatic effects.

With a weak magnetic field electron confinement in the presence of space-charge electric fields determines the sheath width. We can apply results from Section 8.1. We want to find the size of orbits for electrons in a magnetic field B_o subject to a voltage of about $V_o \sim kT_i/e$. From Eq. (8.11) the magnetic sheath width is roughly

$$\lambda_M \sim (2kT_i m_e)^{1/2}/eB_o. \tag{11.60}$$

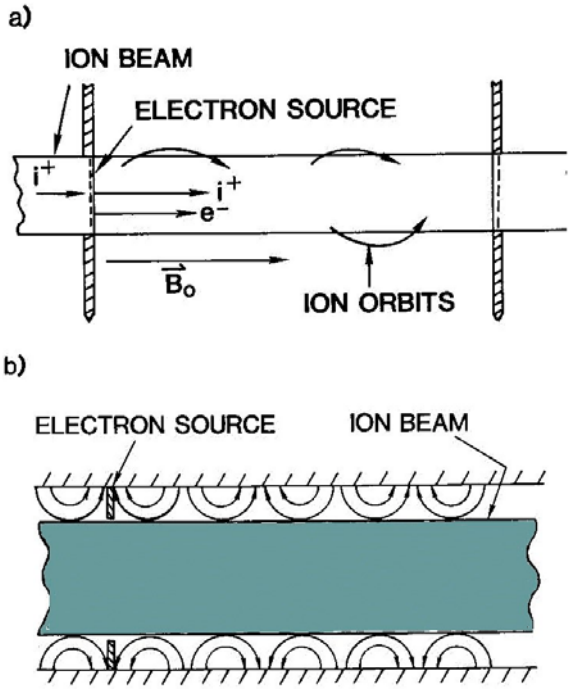

Figure 11.15. Transport of high-intensity neutralized ion beams by the control of electrons. *a*) Weak solenoidal magnetic field confines electrons, while the space-charge electric field confines ions. *b*) Multipole magnetic fields concentrated at the boundary confine neutralizing electrons.

Figure 11.16 shows plots of the electric and magnetic sheath dimensions as functions of kT_i, n_i and B_o. The condition $\lambda_M \gg \lambda_E$ defines the weak magnetic field regime. In an intermediate regime the expansion width for the ions equals the larger of λ_E and λ_M.

As an example suppose we have a neutralized beam of C^+ ions with current density $j_i = 1 \times 10^4$ A/m^2, kinetic energy 2 MeV, and density $n_i = 1.1 \times 10^{16}$ m^{-3}. The beam has an angular divergence of 0.5° corresponding to a transverse temperature of $kT_i = 150$ eV. Equation (11.59) predicts that the electrostatic sheath width is only 0.87 mm. To ensure that $\lambda_M < \lambda_E$, the magnetic field should be $B_o > 0.048$ tesla. The results show that low magnetic fields can confine energetic ion beams through charge-separation effects.

The system of Figure 11.15*a* is impractical for high-flux beams because of the entrance mesh. Also extraction of the neutralized ion beam from the magnetic field is difficult. Figure 11.15*b* shows an alternative geometry for collective ion beam transport. The applied magnetic field is a cusp array (Section 10.9). Magnetic windings with alternate polarity or permanent magnets line the wall of the transport chamber. The axial length of cells is smaller than the coil radius. The resulting cusp field is concentrated at the wall and is small on the axis. Although the weak magnetic fields have little effect on the ions, they strongly focus the neutralizing electrons. The radial electric fields generated by charge separation confine the ions. The cusp array has advantages over the solenoid: 1) the minimum-*B* field provides stable confinement of the low-

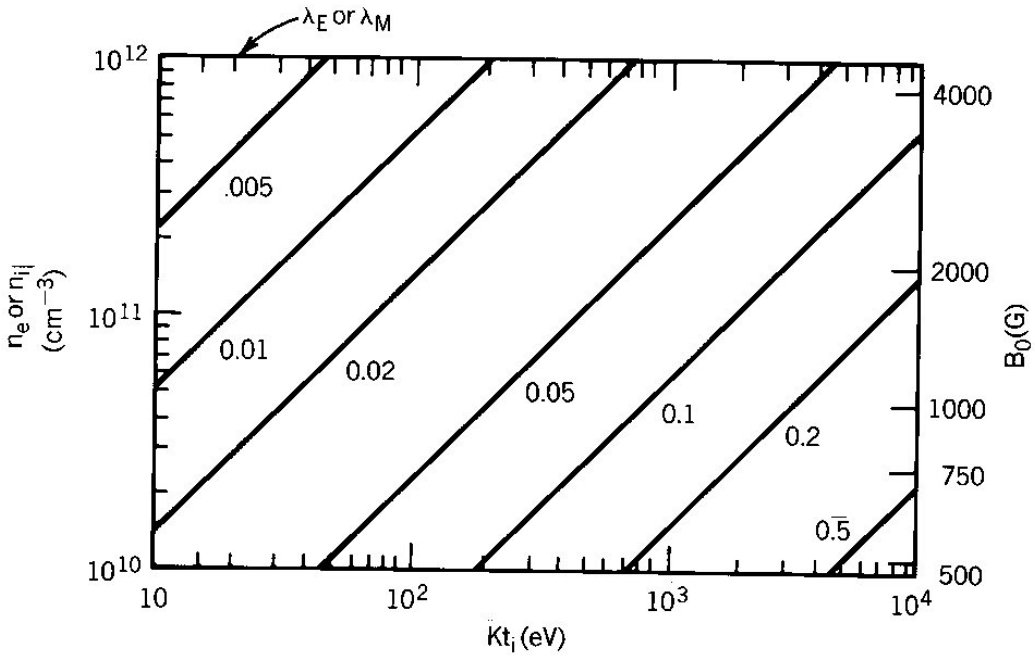

Figure 11.16. Sheaths for electron control of intense neutralized ion beam transport - dimensions in cm. λ_M, the scale length for magnetic confinement of electrons, depends on B_o (kG) and T_i (eV). λ_E, the scale length for electostatic confinement of ions, depends on T_i (eV) and n_i (cm^{-3}).

energy electrons, 2) the neutralized ion beam emerges from and travels to field-free regions. The *space-charge lens* is another option for collective focusing of neutralized ion beams. In contrast to the cusp transport system, the space-charge lens is an isolated solenoid lens with linear radial forces that focus a neutralized ion beam toward a point. To analyze its effect we shall use of the geometry of Figure 11.17. An ideal neutralized beam enters a weak solenoid lens. The ions and electrons of the incident beam have only axial velocity. The density and velocity of the electrons exactly equals that of the ions. The magnetic field of the lens has little effect on the energetic ions – without space-charge electric fields single ions would pass through with little deflection. On the other hand the converging magnetic field lines exert a radial force on the electrons. Compression of the electron distribution creates electric fields that point toward the axis.

To calculate electric fields in the space-charge lens we must find a self-consistent beam equilibrium. For a first order treatment, we neglect changes in the ion density and consider a long solenoidal field. All electrons have zero canonical angular momentum and equal total energy:

$$T_e = T_i(m_e/m_i). \tag{11.61}$$

The constraints on the electron distribution are similar to those we used to calculate the Brillouin

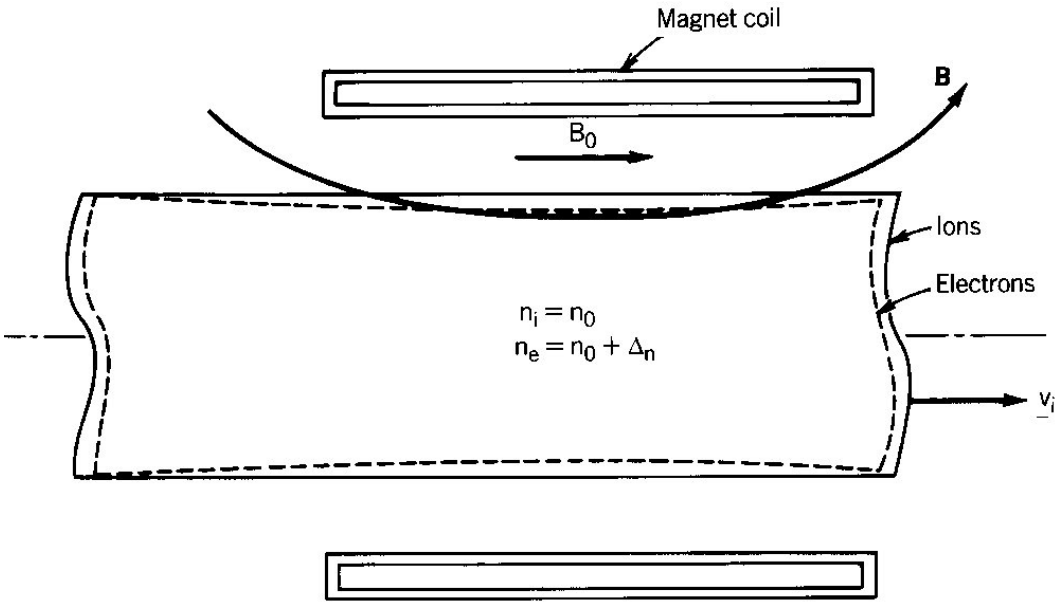

Figure 10.17. Geometry of the space-charge lens.

equilibrium – we can apply the results of Section 10.3. The main difference is the presence of the ions. In the theory of Section 10.3 the charge density n_o represented a bare electron beam. In the space-charge lens the negative charge density arises from an excess of electrons near the axis. We shall denote the negative charge enhancement as Δn. For a high-current neutralized beam, we expect that

$$\Delta n \ll n_i, n_e. \tag{11.62}$$

Section 10.3 showed that Δn is uniform in radius in a self-consistent electron equilibrium. Equation 10.33 implies that the charge imbalance has magnitude

$$\Delta n = (eB_o/2m_e)^2 \, (2\epsilon_o m_e/e^2). \tag{11.63}$$

From Eq. (5.26) the resulting radial electric field is

$$E_r = - \, (\omega_{go}{}^2 m_e/4e) \, r. \tag{11.64}$$

The electric field of Eq. (11.64) combined with the centrifugal force balances the focusing force of the magnetic field so that the neutralizing electrons pass through the lens with small change in radius. The electric field varies linearly with r – the field from the perturbed electrons is independent of the radial variation of ion beam density when the fractional charge imbalance is small.

The space-charge electric force on nonrelativistic ions is much larger than the direct magnetic

force. Within the solenoid lens, the electric force is:

$$F_e = - m_e (eB_o/2m_e)^2 r. \tag{11.65}$$

Equation 9.25 implies that the magnetic force is

$$F_m = - m_i (eB_o/2m_i)^2 r. \tag{11.66}$$

The ratio of forces is:

$$F_e/F_i = (m_i/m_e). \tag{11.67}$$

Equation (11.67) shows that the focusing effect from space separation is over a thousand times stronger than the direct action of the magnetic field.

The space-charge lens has the apparent ability to focus intense ion beams with modest magnetic fields. Unfortunately further analysis shows that a linear force variation is possible only in a restricted parameter regime, limiting applications to low-current ion beams. One restriction is that the magnetic field cannot be so strong that it reflects entering electrons. We discussed this process in Section 10.1. Equation 10.11 gives a constraint on the maximum radius of a neutralized beam:

$$r_b < 2m_e v_i/eB_o. \tag{11.68}$$

To illustrate the implication of Eq. (11.68) suppose we have a 10 MeV C^+ beam with velocity $v_i = 1.26 \times 10^7$ m/s. For a beam radius of 0.02 m, the equation implies that $B_o < 7.2 \times 10^{-3}$ tesla. A neutralized beam can penetrate through a lens with higher applied magnetic field by creating axial space-charge fields that pull electrons through the lens. Although the beam crosses the lens, the associated spread in electron total energy violates the conditions of the model and the radial electric field is non-linear.

With a limit on applied magnetic field we can investigate the constraints imposed by the condition of small fractional change in electron density, Eq. (11.62). From Eq. (11.63) the ratio of the electron density perturbation to the density in the undisturbed beam is

$$\Delta n/n_e = (eB_o/2m_e)^2 (2\epsilon_o m_e/e^2 n_e) \ll 1. \tag{11.69}$$

We can rewrite Eq. (11.69) in a form that shows the limit on the ion beam current,

$$I \ll (\pi/2) (eB_o^2 \epsilon_o v_i/m_e) r_b^2. \tag{11.70}$$

Inserting parameters for the carbon ion beam with $B_o = 5 \times 10^{-3}$ tesla and $r_b = 0.02$ m, we find that $I \ll 0.31$. The implication is that space-charge lenses have linear focusing strength only for low-current ion beams.

To conclude this section, we discuss methods to accelerate neutralized ion beams. The

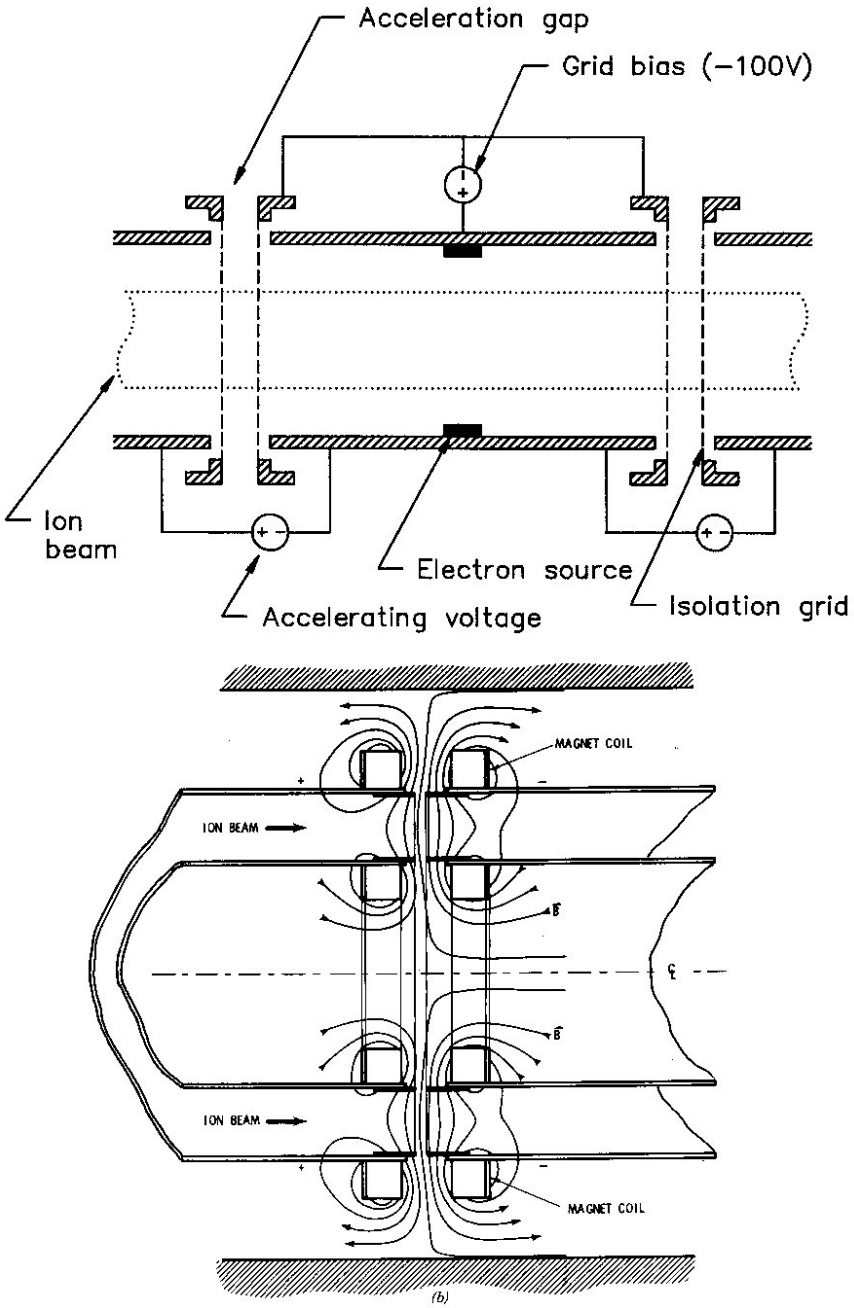

Figure 11.18. Methods to accelerate high-current neutralized ion beams. *a*) Low gradient, large-area injector. Biased grids prevent streaming of electrons into the acceleration gaps. *b*) Radial magnetic field acceleration gap. The magnetic field inhibits electron streaming.

challenge in a neutralized beam accelerator is control of electrons in the presence of strong axial electric fields. The electrons cannot cross acceleration gaps with the ions. The neutralizing electrons must be removed from the ion beam at the entrance to a gap and replaced at the downstream side. Also the drift regions between acceleration gaps must be electrically isolated from the gaps. Accelerating electric fields that penetrate into the drift regions would pull electrons from the neutralized beam and accelerate them backward. Electron loss wastes energy and prevents effective neutralization between gaps. Figure 11.18*a* shows an accelerator for a high-current ion beam that uses grids for electrical isolation of the acceleration gaps. The gap electric field penetrates into the drift region a small distance comparable to the spacing between grid wires. Electron loss is small if the beam in the drift region has a positive potential relative to the grid. In the drift region electrons mix with the ion beam through the transverse neutralization process described in Section 11.2. A beam with a long pulse length traps a distribution of stationary electrons in the drift spaces between narrow acceleration gaps. Shaped grids create transverse components of electric field to focus the ions. The grid accelerator has the disadvantages of ion loss on the grids and degradation of beam emittance by facet lens effects. Nonetheless the device can create high-perveance beams of moderate kinetic energy (~1 MV) and current density (~1×10^4 A/m^2).

The radial magnetic field acceleration gap of Figure 11.18*b* allows acceleration of high-flux neutralized beams. In contrast to the grid accelerator the radial field gap has no physical structure to intercept the beam. Transverse magnetic fields prevent electron flow across the acceleration gaps. The radial field gap is similar to the magnetically insulated gap of Section 8.8 – a pre-accelerated beam replaces the ion source. By conservation of canonical angular momentum the magnetic fields do not contribute a net azimuthal velocity to accelerated ions. For long-pulse beams electrons trapped in the acceleration gap allow enhanced ion flux (Section 8.9). Multiple gap radial field accelerators have generated 3 kA pulsed C^+ beams at 600 keV. Observed current densities of 30×10^4 A/m^2 are well beyond conventional space-charge limits.